An MPD Code with Anomalous Transport*

G. Caldo† E.Y. Choueiri‡ A.J.Kelly§ and R.G. Jahn¶
Electric Propulsion and Plasma Dynamics Laboratory
Princeton University
Princeton, New Jersey 08544, USA

Abstract

A fully two-dimensional, two-fluid numerical code has been specifically developed to study *self-consistently* the effects of anomalous transport on MPD accelerator behavior. The code employs a modified finite-difference MacCormack code for the solution of the two-fluid conservation equations, while concurrently solving the electromagnetic equations via a modified Jacobi method. The main goal of this paper is to demonstrate the self-consistent inclusion of anomalous transport effects in such codes, to compare steady-state spatial distributions of relevant properties in the accelerator with and without anomalous transport and to assess the extent of the impact of plasma turbulence on the overall plasma flow. Anomalous transport theory takes into account the interaction between plasma waves and charged particles due to microinstabilities. Anomalous resistivity and ion heating rate models derived by Choueiri[1] based on the non-linear saturation of the lower hybrid current-driven instability (LHCDI) were used for the calculations and updated self-consistently with the flow at each step in time and space. Polynomial expressions for these rates are presented for inclusion in any two-fluid code. The anomalous rates are important only when the electron drift velocity exceeds a certain threshold (near the ion thermal velocity) and they increase significantly with the electron Hall parameter. The regions near the cathode root, tip and the anode tip were found to be critical for turbulent dissipation.

Nomenclature

$\mathbf{B}$	magnetic field strength
$\mathbf{E}$	electric field
J	total interelectrode current
$\mathbf{j}$	current density
σ	electrical conductivity
ψ	electromagnetic stream function
k	Boltzmann's constant, heat transfer coefficient
m	mass
e	elementary charge
μ_o	permeability of free space
ε_o	permittivity of free space
n	number density
ρ	mass density
p	pressure
T	temperature
E_l	electron-ion energy exchange rate
$\mathbf{v}$	plasma streaming velocity
Ω	electron Hall parameter
ν	collision frequency
r	radial coordinate
z	axial coordinate
t	time
Subscripts	
e	electron
i	ion
n	neutral
h	heavy species
AN	anomalous
eff	effective
t	thermal
d	drift

*This work is supported by the Air Force Office of Scientific Research under contract AFOSR-91-0162 and the National Aeronautics and Space Administration under contract NASA-954997.

†Graduate Student
‡Research Associate
§Senior Research Staff
¶Professor

1 Introduction

During the past ten years, the numerical modeling of MPD accelerators has progressed along with the increased speed and availability of computing fa-

cilities. Together with computational and geometrical improvements, a variety of physical effects have been modeled. Among them, viscosity, heat conduction,and diffusion[2, 3]. The transport coefficients used so far in the calculations are "classical", i.e., they rely on inter-particle collisions and neglect collective effects due to the interaction of particles with unstable oscillations such as those set up by saturated microinstabilities. Furthermore, the charged particles' collision cross-sections employed to calculate ν, k_e, k_h and σ, are usually obtained through simple Coulomb scattering theory that neglects any scattering by turbulent electric and magnetic fields.

In the past five years, much has been learned about the microstability and microturbulence of the MPD accelerator plasma. A recent review of most of the theoretical and experimental work on the subject can be found in ref. [1]. Recent work by Choueiri[4] and Tilley[5, 6] has demonstrated experimentally in both MegaWatt and kiloWatt level accelerators the prevalence of the Generalized Lower Hybrid Drift Instability (GLHDI).

Such microinstabilities are notorious for causing anomalous resistivity (retarding the conduction of electrons through turbulent scattering) and bulk heating of both electrons and ions thus contributing to energy dissipation and possibly erosion in the MPD accelerator. Plasma heating is generally adverse to efficient MPD accelerator operation since typical devices operate at collisional levels where the flow is substantially frozen and enthalpy recovery (electrothermal acceleration) is much less important than electromagnetic acceleration. Enhanced resistivity is also manifested in increased terminal voltage which is in turn reflected in the lowering of thrust efficiency. Numerical codes that include the appropriate anomalous transport may be able to predict more realistically the dissipation, identify regions of the discharge where most dissipation is produced and ideally yield some hints concerning the design of high efficiency, low erosion accelerators. Investigators, working on modeling theta pinch devices (which share many features with the MPD accelerator), for instance, have been very successful in uncovering many aspects of the discharge by self-consistently including anomalous transport in their plasma fluid and hybrid codes[7, 8, 9].

A fundamental problem that arises when trying to include microturbulent effects in a plasma fluid codes is the dichotomy that exists between the microscopic scales of many of the unstable modes and the macroscopic scale of the plasma flow. This fact usually requires that an *a priori* knowledge of the possible microinstabilities must be obtained through theoretical/experimental investigations.

The mathematical description of the microinstabilities combined with that of the corresponding turbulence (through nonlinear theories) would then be interfaced with the fluid code. Three methods for constructing such an interface are discussed in ref. [1]. In this paper we follow the so-called "parameter-specific curve-fit prescription", whereby anomalous heating and momentum exchange rates are calculated from appropriate theories for a wide range of macroscopic parameters that are expected in the calculations. Curve-fits of the results are then made in the multi-parameter space and these curve-fits are then used in each transport update loop of the plasma fluid code. Starting with a general dielectric tensor containing many of the salient physics, it is thus possible to represent the contribution to transport of many unstable modes even if these modes actually evolve and change with the evolving flow.

To-date there has been only one attempt to assess the extent of turbulent dissipation with a numerical flow model. In that work, Hastings and Niewood[10] using a quasi 1-D, one fluid numerical model with *classical* transport calculated the electron-wave momentum exchange frequency $(\nu_e^P)_{AN}$ and the anomalous heating rates of ions and electrons from a quasi-linear description of the modified two stream instability and compared them to classical values. The macroscopic flow parameters used to compute these rates were obtained classically and were thus totally decoupled from the effects of turbulence. In other words, the anomalous rates were not "folded back" into the flow. The study, nonetheless, underscored the importance of anomalous transport in MPD flow models.

Our attempt here can be seen as an improvement on that previous work as we use a fully 2-D, two-fluid code with anomalous transport laws derived using a generalized dispersion tensor that can represent various microinstabilities. Most importantly, the anomalous rates predicted by the flow are folded back into the macroscopic equations at every step in space and time until a self-consistent steady-state is reached.

2 Physical Model

2.1 Geometry

A simple cylindrical geometry with constant cross-section is employed for this study. While this ge-

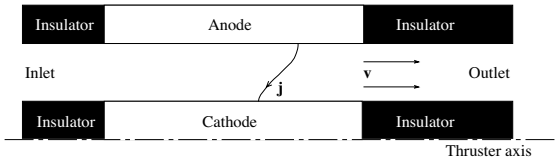

Figure 1: Simplified thruster geometry used for computation.

ometry will, as we shall see, somewhat mute the effects of anomalous transport it has the great benefit of simplicity and a smaller computational burden than more realistic geometries. These will be studied as part of subsequent work. The electrodes were taken to have the same length of 9 cm. Upstream and downstream insulating sections were taken to be aligned with the electrodes and measure, respectively, 3 and 6 cm in length. A cross-section of the chamber is schematically displayed in figure 1.

2.2 Assumptions

A two-fluid, axisymmetric, two-dimensional model has been developed to study the effect of anomalous dissipation on accelerator physics. Electron and heavy species energies, as well as electron and heavy species densities, are separately conserved. Further study of nonequilibrium ionization literature will indicate if more accurate models are necessary. For this study, however, the temperatures are almost always above $1eV$, and the ionization rate and ionization fraction are large independently of the model used.

For wide and short channels such as that of the Full-scale Princeton Benchmark Thruster viscosity might not be a significant effect. For accelerators such as that modeled by Niewood[11], however, finite μ has been shown to significantly affect accelerator efficiency. In this study the flow is assumed to be nonviscous. In future work, viscous effects would be assessed.

Electron-electron and ion-ion heat conduction is included. It is also assumed that each fluid obeys the ideal gas law separately. A Hall term has been introduced in Ohm's law, and no applied magnetic field is assumed.

2.3 Equations

2.3.1 Conservation Laws

The heavy species mass, electron mass, and total momentum conservation equations were expressed in conservative form:

$$\frac{\partial \rho}{\partial t} + \frac{\partial}{\partial z}(\rho v_z) + \frac{\partial}{\partial r}(\rho v_r) = -\frac{\rho v_r}{r}, \tag{1}$$

$$\frac{\partial \rho_e}{\partial t} + \frac{\partial}{\partial z}(\rho_e v_z) + \frac{\partial}{\partial r}(\rho_e v_r) = -\frac{\rho_e v_r}{r} + m_e \dot{n}_e, \tag{2}$$

$$\frac{\partial}{\partial t}(\rho v_z) + \frac{\partial}{\partial z}(\rho {v_z}^2 + p) + \frac{\partial}{\partial r}(\rho v_z v_r) = -\frac{\rho v_r v_z}{r} + j_r B_\theta, \tag{3}$$

$$\frac{\partial}{\partial t}(\rho v_r) + \frac{\partial}{\partial z}(\rho v_z v_r) + \frac{\partial}{\partial r}(\rho {v_r}^2 + p) = -\frac{\rho {v_r}^2}{r} - j_z B_\theta, \tag{4}$$

where $\dot{n}_e$ is calculated using the Hinnov-Hirshberg theory of ionization-recombination[12].

The electron and heavy species energy conservation laws were expressed in terms of the respective pressures:

$$\begin{aligned}\frac{\partial}{\partial t}(\tfrac{3}{2}p_h) + \frac{\partial}{\partial z}(\tfrac{3}{2}p_h v_z) + \frac{\partial}{\partial r}(\tfrac{3}{2}p_h v_r) = &-\frac{5p_h v_r}{2r} \\ &- p_h(\frac{\partial v_z}{\partial z} + \frac{\partial v_r}{\partial r}) + \frac{\partial}{\partial z}(k_h \frac{\partial T_h}{\partial z}) \\ &+ \frac{\partial}{\partial r}(k_h \frac{\partial T_h}{\partial r}) - E_l + (Q_i)_{AN},\end{aligned} \tag{5}$$

$$\begin{aligned}\frac{\partial}{\partial t}(\tfrac{3}{2}p_e) + \frac{\partial}{\partial z}(\tfrac{3}{2}p_e v_{ze}) + \frac{\partial}{\partial r}(\tfrac{3}{2}p_e v_{re}) = &-\frac{5p_e v_{re}}{2r} \\ - p_e(\frac{\partial v_{ze}}{\partial z} + \frac{\partial v_{re}}{\partial r}) + \frac{\partial}{\partial z}(k_e \frac{\partial T_e}{\partial z}) &+ \frac{\partial}{\partial r}(k_e \frac{\partial T_e}{\partial r}) \\ &+ E_l + \frac{{j_r}^2 + {j_z}^2}{\sigma_{eff}}.\end{aligned} \tag{6}$$

where the anomalous heating rate $(Q_i)_{AN}$ and σ_{eff}, the effective conductivity will be defined below in Section 2.3.3.

The heat transfer coefficients are those derived in Mitchner and Kruger[12]. The electron-ion energy exchange rate is

$$E_l = 3\frac{\rho_e}{m_h}\nu_{ei}k(T_e - T_h).$$

The total electron axial and radial speeds are defined as

$$v_{ze} = v_z - \frac{j_z}{en_e}, \qquad v_{re} = v_r - \frac{j_r}{en_e}. \tag{7}$$

2.3.2 Electromagnetic Equation

If we define $\psi = \frac{B_\theta}{r}$, we can write Ampere's law in the form

$$j_z = \frac{1}{\mu_0 r}\frac{\partial \psi}{\partial r}, \qquad j_r = -\frac{1}{\mu_0 r}\frac{\partial \psi}{\partial z}. \tag{8}$$

Ohm's law is

$$j_z = \sigma\left[E_z + \frac{\psi}{r}(v_r - \frac{j_r}{en_e})\right] \tag{9}$$

$$j_r = \sigma\left[E_r - \frac{\psi}{r}(v_z - \frac{j_z}{en_e})\right]. \tag{10}$$

Faraday's law is expressed as

$$\frac{\partial E_r}{\partial z} - \frac{\partial E_z}{\partial r} = 0. \tag{11}$$

Combining equations 8,9,10 and 11, and remembering that **B** is divergenceless, we obtain a single equation in ψ:

$$\frac{\partial^2 \psi}{\partial z^2} + \frac{\partial^2 \psi}{\partial r^2} + \gamma_1 \frac{\partial \psi}{\partial z} + \gamma_2 \frac{\partial \psi}{\partial r} + \gamma_3 \psi = 0, \tag{12}$$

where

$$\gamma_1 = -\frac{1}{\sigma}\frac{\partial \sigma}{\partial r} - \frac{\psi\sigma}{r}\frac{\partial \frac{1}{en_e}}{\partial r} + \frac{2\sigma}{en_e r^2}\psi - \mu_0 \sigma v_z,$$

$$\gamma_2 = -\frac{1}{\sigma}\frac{\partial \sigma}{\partial z} + \frac{\psi\sigma}{r}\frac{\partial \frac{1}{en_e}}{\partial z} - \frac{1}{r} - \mu_0 \sigma v_z,$$

$$\gamma_3 = -\mu_0 \sigma \psi(\frac{\partial v_z}{\partial z} + \frac{\partial v_r}{\partial r} - \frac{v_r}{r}).$$

2.3.3 Anomalous Transport

The anomalous ion heating and electron momentum exchange rate models used in this code are derived by Choueiri[1] from a second-order weak turbulence theory. The theory is based on a generalized fully electromagnetic dispersion tensor that can represent various microinstabilities which may be sustained by a magnetoactive, collisional, finite-beta, flowing and transverse-current carrying plasma. The interested reader is referred to that work for more details.

In general the microstability (and hence microturburlence) description depends on the following set of eight independent macroscopic parameters

$$kr_{ce}, \quad \Psi, \quad \frac{m_i}{m_e}, \quad \frac{\omega_{pe}}{\omega_{ce}}, \quad \beta_e, \quad \frac{u_{de}}{v_{ti}}, \quad \frac{T_i}{T_e}, \quad \frac{\nu_{ei}}{\omega_{lh}} \tag{13}$$

(where T_i is the same as T_h in the flow code). The first two parameters kr_{ce} (r_{ce} being the electron cyclotron radius) and Ψ represent the normalized wavenumber and propagation angle (with respect to the magnetic field) of the oscillations respectively and are varied to growth-maximize the solutions. Since all anomalous transport rates used here were calculated at maximum growth these two parameters drop out of the final models. The mass ratio m_i/m_e is that of argon. All solutions were found to be very insensitive to the fourth parameter, namely the ratio of electron plasma frequency to the electron cyclotron frequency ω_{pe}/ω_{ce}, as long as that ratio exceeded 10 which was the case for all our simulations. Similarly, the solutions were weakly dependent on β_e (the ratio of electron thermal pressure to magnetic pressure) as long as the electron Hall parameter did not exceed 10. Although that was the case for our numerical simulations reported below, it is expected that the simulation of more realistic geometries at high total currents would raise the electron Hall parameter enough to require the full inclusion of finite-beta effects.

The last three parameters are the most important for our problem. First, u_{de}/v_{ti} must reach a threshold for the instability to be excited and hence for anomalous transport to be operative. For the entire region of parameter-space considered in the simulations that threshold was very near 1.5. Second, the ion to electron temperature ratio plays a role in scaling the level of turbulence. Invariably for our parameter-space, it was found that increasing T_i/T_e causes a devaluation of anomalous transport. The most important of all the macroscopic parameters turned out to be the last one namely ν_{ei}/ω_{lh} where ω_{lh} is the lower hybrid frequency. Indeed this parameter can be replaced by the electron Hall parameter Ω since

$$\Omega \equiv \frac{\omega_{ce}}{\nu_{ei}} = \frac{(m_i/m_e)^{1/2}}{\nu_{ei}/\omega_{lh}}. \tag{14}$$

The calculated anomalous resistivity from the above mentioned theories[1]

$$\eta_{AN} \equiv \frac{m_e(\nu_e^P)_{AN}}{e^2 n_e} \tag{15}$$

normalized by its classic counterpart $\eta_{Cl} \equiv m_e\nu_{ei}/e^2 n_e$ is shown in Fig. (2). It is important to

[1]The weak turbulence theory calculations of the anomalous rates required the knowledge of the saturation energy density of the fluctuations. A model based on saturation by ion trapping was used. Accurate description of the saturation mechanism is still pending particle simulation of the relevant instabilities. For a detailed discussion of other possible saturation mechanisms such as electron trapping, resonance broadening and wave-wave coupling as well as a description of the adopted ion trapping saturation model see ref. [1].

note that an increase in the electron Hall parameter for typical values of T_i/T_e leads to a very significant increase in the anomalous resistivity *if* the parameter u_{de}/v_{ti} is above the stability threshold. It is interesting to note that the scaling of this ratio with the Hall parameter is in general agreement with that recently inferred by Gallimore[13] from measurements in the anode region.

A similar plot is shown in Fig. (3) for the ion heating rate $(\nu_i^T)_{AN}$ normalized by the Coulomb frequency.

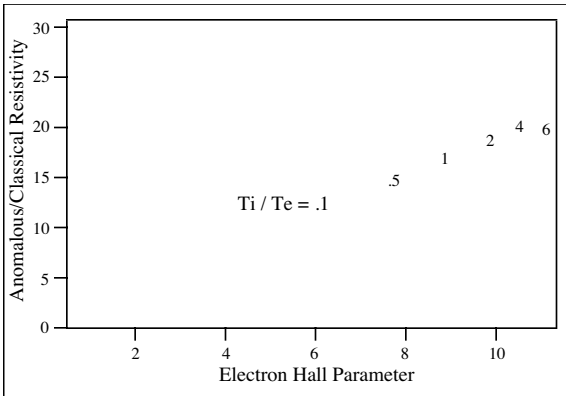

Figure 2: Ratio of anomalous resistivity to classical resistivity as a function of the electron Hall parameter and T_i/T_e with u_{de}/v_{ti} exceeding 1.5,

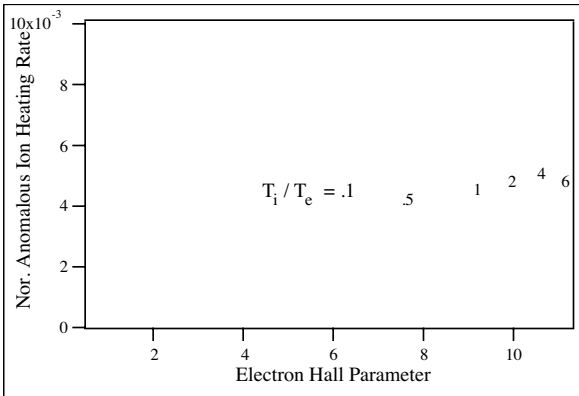

Figure 3: Anomalous ion heating rate normalized by the Coulomb frequency as a function of the electron Hall and T_i/T_e with u_{de}/v_{ti} exceeding 1.5

The above calculated rates and their dependences are included in the flow code. The frequency $(\nu_e^P)_{AN}$ contributes to the anomalous resistivity which in turn, through the Joule heating term in Eq. (6), enhances the electron heating rate. The anomalous ion heating rate represents the time rate of ion bulk heating due to turbulence.

A two-parameter, variable cross-term, least square fit was made to the calculated rates shown in Figs. (2) and (3) in order to include them in the flow code.

The resulting two-parameter interpolating polynomial for $(\nu_i^T)_{AN}/\nu_{ei}$ has an average accuracy of 15% and reads

$$\begin{aligned}\frac{(\nu_i^T)_{AN}}{\nu_{ei}} &= 5.36\times10^{-5} + 1.29\times10^{-5}\ \Omega \\ &\quad + 6.03\times10^{-6}\ \Omega^2 + 9.44\times10^{-8}\ \Omega^3 \\ &\quad + \frac{T_h}{T_e}(-7.55\times10^{-7} - 5.41\times10^{-6}\ \Omega \\ &\quad - 3.93\times10^{-6}\ \Omega^2). \end{aligned} \tag{16}$$

The ions are heated by the turbulent fluctuations at a rate $(Q_i)_{AN} = \frac{3}{2}(\nu_i^T)_{AN}T_h$

The effective conductivity introducing the anomalous resistivity effect to the flow code has the form

$$\sigma_{eff} = \frac{e^2 n_e}{m_e(\nu_{ei} + (\nu_e^P)_{AN})}, \tag{17}$$

where $(\nu_e^P)_{AN}$ is the electron-wave momentum exchange frequency, which is again computed through an interpolating polynomial of average accuracy of 10%

$$\begin{aligned}\frac{(\nu_e^P)_{AN}}{\nu_{ei}} &= 0.192 + 3.33\times10^{-2}\ \Omega + .212\Omega^2 \\ &\quad - 8.27\times10^{-5}\ \Omega^3 + \frac{T_h}{T_e}(1.23\times10^{-3} \\ &\quad - 1.58\times10^{-2}\ \Omega \\ &\quad - 7.89\times10^{-3}\ \Omega^2). \end{aligned} \tag{18}$$

At all the gridpoints where $u_{de}/v_{ti} < 1.5$ both, $(\nu_e^P)_{AN}$ and $(\nu_i^T)_{AN}$ are set to zero and all transport is assumed purely classical. Otherwise, the anomalous rates are computed from the above polynomials using the instantaneous macroscopic parameters and folded back into the flow equations at every time step thus insuring self-consistency.

2.4 Boundary Conditions

At the inlet, the heavy species temperature is fixed to 10^4K, the mass flow rate to $6g/s$, and the Mach number to 1. The electron temperature, furthermore, is

taken to satisfy $\partial T_e/\partial z = 0$ at $z = 0$. The radial velocity is set to 0. The total current J is $16KA$, which specifies the value of the stream function to $\psi = 4\pi J/\mu_o = 3.2 \times 10^{-3}$ T/m. The fluid velocity is determined from the Mach number and the heavy species temperature. The inlet density is taken to be uniform and such that $2\pi \int_r \rho v_r r dr = \dot{m}$. The ionization ratio is taken so as to make $\dot{n}_e = 0$, i.e. there is no net electron production at the inlet.

The heavy species temperature at the walls is again set to $10^4 K$, and the electron normal derivative is zero. The radial velocity is zero.

At the upstream insulators ψ is equal to the inlet value, while at the downstream insulator and at the outlet it is set to zero. At outflow, the axial derivatives of p_e, p_h, ρ, ρ_e, and v_z are set to zero.

3 Numerical Methods

The flow field code uses a modified MacCormack technique first used by Jacoby for laser applications[14]. This is a second-order explicit finite-difference code which yields a steady-state flow solution.

The solution of the conservation equations through the MacCormack routine is alternated with the solution of the electromagnetic equation, until consistency among all the parameters is achieved.

The stream function equation 12 is solved with a second-order nonlinear explicit scheme developed at EPPDyL . After a central difference discretization is performed, equation 12 assumes the form

$$\zeta_1 \psi_{ij} + \zeta_2 = 0. \tag{19}$$

Here ψ_{ij} stands for the value of ψ at the i^{th} horizontal and j^{th} vertical discrete steps. The coefficients ζ_1 and ζ_2, then, are functions of the differential equation's coefficients and of $\psi_{i-1,\,j}$, $\psi_{i+1,\,j}$, $\psi_{i,\,j-1}$, $\psi_{i,\,j+1}$ Each iteration step we set

$$(\psi_{ij})^{(n+1)} = -\left(\frac{\zeta_2}{\zeta_1}\right)^{(n)}, \tag{20}$$

until $(\psi_{ij})^{(n+1)}/(\psi_{ij})^{(n)}$ is equal to 1. Using as initial guess the value of ψ computed at the previous MacCormack step, convergence is achieved in a number of steps ranging between 1 and 250.

4 Results

For a thruster with $\dot{m} = 6g/s$ and $J = 16KA$, the code was run to steady-state both with and without the two anomalous transport correction terms mentioned above.

As mentioned above, an anomalous correction on the resistivity was added only at those points where $u_{de}/v_{ti} \geq 1.5$. Figure 4 illustrates the range of variation of this dimensionless parameter. Anomalous corrections were thus automatically applied for regions near the root and tip of the cathode and the tip of the anode. Since u_{de}/v_{ti} is proportional to the current density, it is expected that increasing J (or more accurately $J^2/\dot{m}$) will have the effect of expanding the areas where anomalous corrections are applied. Furthermore, for geometries such as that of the Benchmark Thruster, where the current density is very high along a segment of the anode, anomalous corrections to transport will be relevant also in this region.

As figures 2 and 3 show, the anomalous frequencies strongly increase for a higher electron Hall parameter. The electron Hall parameter Ω is therefore a very good indicator of where the differences between the classical and the anomalous case will occur. Figure 5 illustrates the variation of Ω in this thruster geometry. Of course, only in the regions where u_{de}/v_{ti} exceeds its threshold will any corrections be added. It is therefore important to observe how Ω varies *within* those regions. Figure 6 shows this variation, again emphasizing that the regions near the cathode tip and root and the anode tip are the most critical from the standpoint of anomalous dissipation. Hall parameter distribution, however, is a strong function of geometry, and for any but the simplest thruster configuration, there are going to be ample regions in which Ω is going to extend well above its present maximum of 3.2.

The differences between "anomalous" and "classical" configurations obtained in this study, although substantial, are therefore expected to be far larger for real "open" thruster geometries with higher $J^2/\dot{m}$ since in such situations u_{de}/v_{ti} will exceed its threshold over a larger portion of the grid and the higher electron Hall parameters would invariably lead to more substantial turbulent dissipation.

Enclosed current lines are shown in figure 7. The current bulges at the tip of the electrodes, as is consistent with previous numerical results[2, 15]. No significant differences in the current distribution were found between the two cases.

As is apparent from equation 17, the anomalous corrections reduce the value of the conductivity. Figure 8 shows the ratio of the conductivity from the classical run to that obtained from the simulation

containing anomalous transport. It is again apparent that this decrease is greatest near the root of the cathode, as is expected. It is interesting to note from that figure that in some parts of the discharge away from the critical regions, the ratio of the conductivities can drop below unity. This can be explained as follows. While the anomalous resistivity effect is localized to the critical regions, enhanced electron heating due to turbulence can spread from these critical regions and raise the electron temperature, thus in turn raising the Coulomb conductivity over what it would be, had the transport been purely classical.

Another finding of this study is the sensible increase in the heavy species (ion) temperature for the anomalous run. As figure 9 illustrates, next to the cathode root and tip the ratio of the ion temperature obtained from the anomalous transport run to that obtained from classical simulation is as high as 1.58. this corresponds to an increase in temperature of 7000-8000 K.

It is interesting to note in this context that the cathode root region, which, according to the above results is most affected by turbulent heating and dissipation, has long been known to play an important role in thruster component longevity. Aside from the erosion of the cathode root itself, the center of the insulating injection backplate in real thrusters, which would be directly exposed to this microturbulent region of the discharge, is well established to be a critical region for ablation. It is most interesting to remark that the backplate erosion measurements of Rowe[16] and Ho[17] clearly indicate that the ablation of the backplate happens near the cathode root and is greatly enhanced when "instabilities" appear in the voltage signature[16].

The "shifting" of the plasma heating region towards the cathode tip due to anomalous effects becomes even more apparent when comparing Fig. (10) to Fig. (11) representing the ratio T_i/T_e for the classical and anomalous simulations respectively. Microturbulent effects also raise the maximum magnitude of that ratio as is apparent from the same plots.

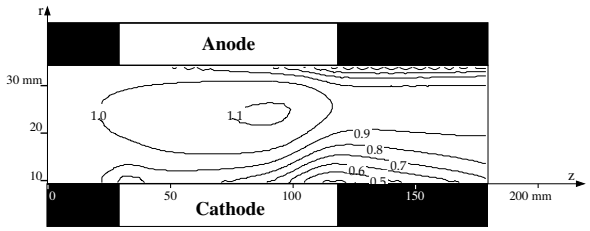

Figure 10: Ratio of heavy species temperature to electron temperature for classical transport run.

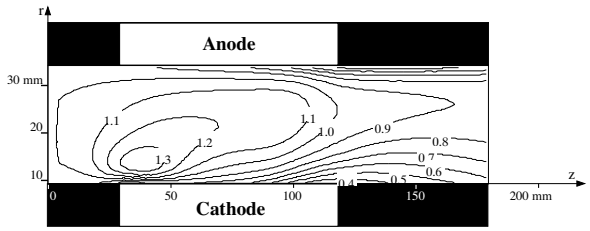

Figure 11: Ratio of heavy species temperature to electron temperature for anomalous transport run.

5 Summary

A two-fluid, two-dimensional finite-difference code was developed to model plasma flow with self-consistent anomalous transport in an MPD accelerator. The code employs a combination of a modified MacCormack and a modified Jacobi method to solve the plasma fluid equations for steady-state. The anomalous transport is calculated at each time and space step using models for momentum exchange and heating rates due to particle scattering by microturbulence. For anomalous dissipation to be operative at all in a region of the discharge, the electron drift velocity, u_{de}, must exceed a threshold about the ion thermal velocity in that region. Once anomalous transport is operative in a certain region, microturbulent dissipation (plasma heating and anomalous resistivity) is strongly enhanced with increasing electron Hall parameter and to a lesser extent with decreasing T_i/T_e. The anode and cathode tip regions and most particularly the cathode root region were found to be most prone to microturbulent dissipation. The enhanced dissipation is expected to be even more dramatic for real "open" thruster geometries operating at higher $J^2/\dot{m}$ since for such cases u_{de}/v_{ti} will exceed its threshold more widely and the larger electron Hall parameters would invariably lead to more substantial turbulent dissipation.

References

[1] E.Y. Choueiri. *Electron-Ion Streaming Instabilities of an Electromagnetically Accelerated*

Plasma. PhD thesis, Princeton University, Princeton, NJ, USA, 1991.

[2] P. C. Sleziona, M. Awter-Kurtz, and H. O. Shrade. Numerical evaluation of MPD thrusters. In 21^{st} *International Electric Propulsion Conference*, Orlando,Florida, 1990. AIAA-90-2602.

[3] S. Miller and M. Martinez-Sanchez. Viscous and diffusive effects in MPD flows. In 21^{st} *International Electric Propulsion Conference*, Orlando,Florida, 1990. AIAA-90-2606.

[4] E.Y. Choueiri, A. J. Kelly, and R. G. Jahn. Current-driven plasma acceleration versus current-driven energy dissipation part II : Electromagnetic wave stability theory and experiments. In 22^{nd} *International Electric Propulsion Conference*, Viareggio, Italy, 1991. IEPC-91-100.

[5] D.L. Tilley. An investigation of microinstabilities in a kW level self-field MPD thruster. Master's thesis, Princeton University, Princeton, NJ, USA, 1991.

[6] D.L. Tilley, E.Y. Choueiri, A.J. Kelly, and R.G. Jahn. An investigation of microinstabilities in a kW level self-field MPD thruster. In 22^{nd} *International Electric Propulsion Conference*, Viareggio, Italy, 1991. IEPC-91-122.

[7] P.C. Liewer and N.A. Krall. Self-consistent approach to anomalous resistivity applied to theta pinch experiments. *Physics of Fluids*, 16(11):1953–1963, 1973.

[8] R.C. Davidson and N.A. Krall. Anomalous transport in high-temperature plasmas with applications to solenoidal fusion systems. *Nuclear Fusion*, 17(6):1313–1372, 1977.

[9] S. Hamasaki, N.A. Krall, C.E. Wagner, and R.N. Byrne. Effect of turbulence on theta pinch modeling by hybrid numerical models. *Physics of Fluids*, 20:65–71, 1977.

[10] D. Hastings and E. Niewood. Theory of the modified two stream instability in an MPD thruster. In 25^{th} *Joint Propulsion Conference*, Monterey, CA, USA, 1989. AIAA-89-2599.

[11] E. Niewood. Transient one-dimensional simulation of magnetoplasmadynamic thrusters. Master's thesis, Massachusetts Institute of Technology, 1989.

[12] M. Mitchner and C.H. Kruger. *Partially ionized Gases*. Wiley Interscience, New York, 1973.

[13] A.D. Gallimore, A. J. Kelly, and R. G. Jahn. Anode power deposition in MPD thrusters. In 22^{nd} *International Electric Propulsion Conference*, Viareggio, Italy, 1991. IEPC-91-125.

[14] H. Jacoby. Entwicklung eines teoretischen modells zur beschreibung der wechselwirkung zwischen elektrischer entladung und uberschallstromung eines gepulsten co-lasers. Master's thesis, Institut fur Technische Physik, Stuttgart, 1984.

[15] M. R. LaPointe. Numerical simulation of self-field MPD thrusters. In 27^{th} *Joint Propulsion Conference*, Sacramento, CA, 1991. AIAA 91-2341.

[16] R. A. Rowe. Ablation of an MPD thruster. Master's thesis, Princeton University, Princeton, NJ, USA, 1981.

[17] D.D. Ho. Erosion studies in an MPD thruster. Master's thesis, Princeton University, Princeton, NJ, USA, 1981.